Optimal Selection of the Average Capacitor Voltage for Variable-Speed Drives With Modular Multilevel Converters

Antonios Antonopoulos, *Student Member, IEEE,* Lennart Ängquist, *Member, IEEE,*
Lennart Harnefors, *Senior Member, IEEE,* Hans-Peter Nee, *Senior Member, IEEE*

***Abstract*—Variable-speed drives have reduced voltage requirements when operating below the base speed. In a modular-multilevel-converter-based (M2C-based) motor drive it is then possible to operate with reduced voltage in the submodule capacitors, than at the base speed. In this sense, a greater capacitor-voltage ripple can be accommodated, without exceeding the maximum peak-capacitor voltage. This paper presents an analytical investigation for the optimal selection of the average capacitor voltage for M2Cs, when the motor is operating with rated torque, below the base speed. This method does not require any power exchange between the converter arms, so it keeps the conduction losses at the minimum level. Additionally, the method decreases the switching losses, due to the decreased capacitor-voltage level. The overall ratings of the converter remain the same as in the base-speed operation. It is shown that this method can be applied at a speed range between the base speed and down to approximately one third of it, i.e, an operating range that covers the requirements for typical pump- and fan-type applications. The results obtained from the analytical investigation are experimentally verified on a down-scaled laboratory prototype M2C.**

***Index Terms*—Capacitor-voltage control, medium-power variable-speed drives, modular multilevel converters, optimization.**

I. Introduction

THE MODULAR MULTILEVEL CONVERTER (M2C), outlined in Fig. 1, was first presented by Marquardt and Lesnicar [1], [2], and has recently attracted a lot of interest in various applications [3]–[8]. It has been suggested to be used for high-power motor drives [9]–[11]. A common requirement for many motor-drive applications is full-torque operation in a variable-speed range, even from zero to base speed. This is, however, a far more complex task with an M2C than if a conventional voltage-source converter with two or three levels is used. Presently, no M2C control method has been presented that can be used in the entire speed range. Moreover, a considerable over-rating of the M2C is required in variable-speed applications according to [12], even if several measures are taken to reduce it. In [13] it was shown that different control methods could be used in different speed ranges such that the whole speed range from zero to base speed could be handled. In the low-speed range (approximately 0-0.1 p.u.) the main issue is to balance the voltages of the upper and lower arms [14]. This is achieved by adding a higher-order common-mode voltage to the arm voltages, and by driving a circulating current of the same frequency, such that a power flow between the upper and lower arms is obtained [11], [15]. In the intermediate frequency range (approximately 0.1-0.3 p.u.) the main obstacle is to minimize the voltage ripple of the submodule capacitors. This is a complicated task involving addition of several frequency components in the circulating current, and the solution can be considered as a trade-off between the voltage and current ratings of the components. Above that region and up to the base speed (approximately 0.3-1.0 p.u.), it is sufficient to reduce the average voltage of the submodule capacitors in order to accommodate for the voltage ripple created by the rated fundamental current.

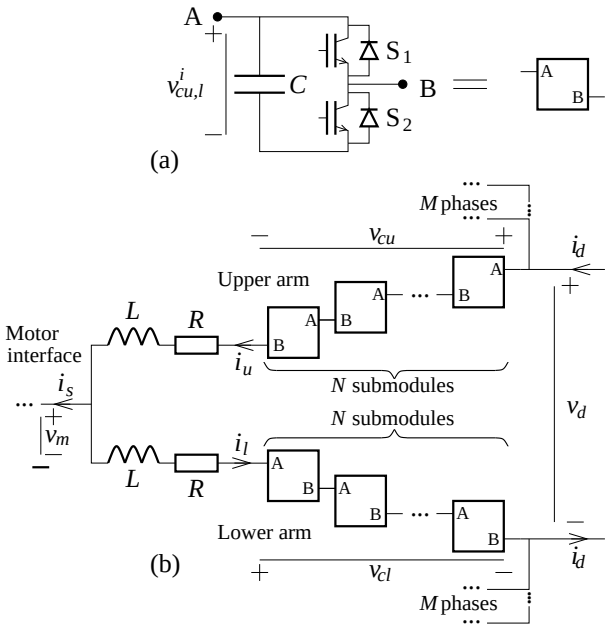

Fig. 1. Outline of the basic topology of an M2C.

The aim of this work is to discuss the possibility of making an analytical optimization of the average capacitor voltage of an M2C in the widest of the above operating regions, i.e, the high-speed range (from 0.3 to 1.0 p.u.). The benefits or this

This paper was presented at the IEEE Energy Conversion Congress & Exposition (ECCE) in Denver, CO, USA September 15-19, 2013

A. Antonopoulos, and L. Harnefors are with ABB Corporate Research, Västerås, Sweden, and also with the KTH Royal Institute of Technology, 100 44 Stockholm, Sweden (e-mail: antonios.antonopoulos@se.abb.com, lennart.harnefors@se.abb.com).

L. Ängquist, and H.-P. Nee are with the Electrical Energy Conversion Laboratory (E2C), KTH Royal Institute of Technology, 100 44 Stockholm, Sweden (e-mail: tlan@kth.se, hansi@kth.se).

optimization are the following:

- The increased voltage ripple caused by the low-frequency current does not result in overrating the submodule components.
- Unlike [16], no oscillating component is injected in the circulating current to shape the capacitor voltages, and therefore, no additional conduction losses are created.
- The switching losses are reduced, as the capacitor voltage that is switched in or out is reduced on average.
- The output-current waveform is not distorted, as all the available voltage is used. This is due to the fact that all the available levels appear in the line-line voltage waveform, even if the request for magnetizing voltage decreases proportionally with the speed.

The question that is answered with this study is how much is it possible to decrease the average capacitor voltage before the available arm voltage is no longer sufficient to achieve the desired inserted voltage. In order to determine exactly when this occurs, the margin between the available and the inserted arm voltage is investigated, identifying the conditions which are minimizing it.

The control method used in this study is briefly discussed in Section II. The analytical study concerning the available arm voltage and the optimization of its average value is shown in Section III. Operating points derived from the analytical investigation are experimentally confirmed in Section IV. A discussion about the advantages of this method is carried out in Section V, before the final conclusions are presented.

II. M2C Internal Control

The control method that is utilized in this paper is established in [17]. An outline of the controller is given in Fig. 2. The internal control is operating in open loop, meaning that the

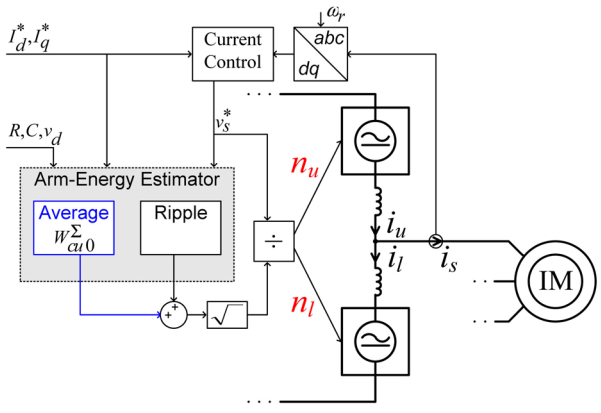

Fig. 2. Block diagram describing the internal control of the M2C. The algorithm described in this paper is estimating the minimum average in the arm energy (i.e., $W_{cu,l0}^{\Sigma}$-blue block).

output voltage reference is calculated based on estimations for the internal states of the converter, rather than measurements. This is favorable in the sense that measurement related effects, such as delays, are avoided, while the stability of the converter system is not compromised [18]. A closed-loop system has, moreover, a more complicated design, as special care should be taken when estimating gains and tuning filters for variable-frequency operation [19], [20]. On the other hand, a well-tuned feedback design can offer faster dynamic response.

The output-current controller is, for that reason, necessary to operate always in closed loop. Relying on a sufficiently effective current controller, the output alternating current is assumed to be a pure sinusoid

$$i_s = \hat{I}_s \cos(\omega_s t - \varphi), \tag{1}$$

and the references for the inserted arm voltages are

$$v_{cu,l} = \frac{v_d}{2} \mp \hat{V}_s \cos\omega_s t - R i_{c0}. \tag{2}$$

With a constant dc-link voltage, the direct component in the circulating current is estimated from the instantaneous power exchange between the dc and ac sides, using the purely sinusoidal output current in (1), and the references for the inserted voltages from (2), as

$$i_{c0} = \frac{\hat{V}_s \hat{I}_s \cos\varphi}{v_d + \sqrt{v_d^2 - 4R\hat{V}_s\hat{I}_s\cos\varphi}} \approx \frac{\hat{V}_s\hat{I}_s\cos\varphi}{2v_d}. \tag{3}$$

For a constant circulating current, it can be shown [17], [18] that the variations of the stored energies in the upper and lower arms are given by

$$\begin{aligned} W_{cu,l}^{\Sigma} = W_{cu,l0}^{\Sigma} &\mp \frac{\hat{V}_s i_{c0}\sin(\omega_s t)}{\omega_s} \\ &\pm \frac{(\frac{v_d}{2} - R i_{c0})\hat{I}_s \sin(\omega_s t - \varphi)}{2\omega_s} \\ &- \frac{\hat{V}_s\hat{I}_s\sin(2\omega_s t - \varphi)}{8\omega_s}, \end{aligned} \tag{4}$$

which can be used to calculate the final insertion indices, as

$$v_{cu,l}^{\Sigma} = \sqrt{\frac{2NW_{cu,l}^{\Sigma}}{C}} \Rightarrow n_{u,l} = \frac{v_{cu,l}}{v_{cu,l}^{\Sigma}}. \tag{5}$$

The terms $W_{cu,l0}^{\Sigma}$ are integration constants. As mentioned in [17], [18], the latter can be freely selected, and are the mean values for the available energy stored in the arms. *The focus of this study is on these constants, and the question that is answered here is what is the optimal value in order to have sufficient available energy stored in the arms to provide the desired instantaneous value of the inserted arm voltage.*

III. Available-Arm-Energy Margin

A. Time-Domain Expression

In order to determine the margin between the available arm energy and the desired inserted arm voltage, both quantities have to be measured with the same units, i.e., the inserted voltage needs to be expressed as an "inserted arm energy" value. This is done in a similar way as in [19], [20]. Getting the inserted arm voltage from (2), the inserted arm energy can be calculated as

$$\begin{aligned} W_{cu,l} =& \frac{C}{2N} v_{cu,l}^2 = \frac{C}{2N}\left(\frac{v_d}{2} \mp \hat{V}_s\cos(\omega_s t) - R i_{c0}\right)^2 \\ =& \frac{C}{2N}\left[\left(\frac{v_d}{2} - R i_{c0}\right)^2 + \hat{V}_s^2\cos^2(\omega_s t)\right. \\ & \left. \mp (v_d - 2R i_{c0})\hat{V}_s\cos(\omega_s t)\right]. \end{aligned} \tag{6}$$

Subtracting (6) from (4), substituting $\omega_s t \to \theta$, and reformulating to remove the multiple-frequency terms, the available-arm-energy margin as a function of the argument θ is given as

$$\begin{aligned}\Delta W_{cu,l} =& W^{\Sigma}_{cu,l} - W_{cu,l}\\ =& \underbrace{W^{\Sigma}_{cu,l0} - \frac{C}{8N}\left(v_d - 2Ri_{c0}\right)^2 - \frac{\hat{V}_s\hat{I}_s}{8\omega_s}\sin\varphi}_{f}\\ &+ \underbrace{\left(\frac{N\hat{V}_s\hat{I}_s\sin\varphi - 2\omega_s C\hat{V}_s^2}{4N\omega_s}\right)}_{a}\cos^2\theta\\ &\pm \underbrace{\left(\frac{\left(v_d - 2Ri_{c0}\right)\hat{I}_s\cos\varphi - 4\hat{V}_s i_{c0}}{4\omega_s}\right)}_{2e}\sin\theta\\ &\pm \underbrace{\left(v_d - 2Ri_{c0}\right)\left(\frac{2\omega_s C\hat{V}_s - N\hat{I}_s\sin\varphi}{4N\omega_s}\right)}_{2d}\cos\theta\\ &\underbrace{-\frac{\hat{V}_s\hat{I}_s\cos\varphi}{4\omega_s}}_{2b}\cos\theta\sin\theta. \end{aligned} \tag{7}$$

Both the available and the inserted arm energy contain a term varying with twice the fundamental frequency; this indicates that there may exist up to two minimum and two maximum points in one fundamental period. The arguments of these local minima and maxima can be found by differentiating (7) with respect to θ and setting this derivative to zero, as in

$$\begin{aligned}\frac{d\Delta W_{cu,l}}{d\theta} =& 2b\cos^2\theta - 2a\cos\theta\sin\theta - 2b\sin^2\theta\\ &\pm 2e\cos\theta \mp 2d\sin\theta = 0. \end{aligned} \tag{8}$$

B. Geometrical Interpretation

Replacing $\cos\theta \to x$ and $\sin\theta \to y$, (8) is translated into the $(\cos\theta, \sin\theta)$ coordinate system as

$$H(x,y) = 2bx^2 - 2axy - 2by^2 \pm 2ex \mp 2dy = 0, \tag{9}$$

which forms a quadratic equation. This equation represents a conic section, and the sought minima and maxima of (7) are the crossing points of (9) with the unit circle $x^2 + y^2 = 1$, which represents the $x - y$ relation, in the $(\cos\theta, \sin\theta)$ coordinate system. The general expression of the quadratic equation for the available-arm-energy-margin derivative can then be expressed in the form

$$H(x,y) = Ax^2 + 2Bxy + Cy^2 + 2D_{u,l}x + 2E_{u,l}y + F = 0 \tag{10}$$

with

$$\left\{\begin{array}{l} A = 2b = -\frac{\hat{V}_s\hat{I}_s\cos\varphi}{4\omega_1}\\ B = -a = -\frac{N\hat{V}_s\hat{I}_s\sin\varphi - 2\omega_1 C\hat{V}_s^2}{4N\omega_1}\\ C = -2b = \frac{\hat{V}_s\hat{I}_s\cos\varphi}{4\omega_1}\\ D_{u,l} = \pm e = \pm\frac{\left(v_d - 2Ri_{c0}\right)\hat{I}_s\cos\varphi - 4\hat{V}_s i_{c0}}{8\omega_1}\\ E_{u,l} = \mp d = \mp\left(v_d - 2Ri_{c0}\right)\frac{2\omega_1 C\hat{V}_s - N\hat{I}_s\sin\varphi}{8N\omega_1}\\ F = 0 \end{array}\right\}. \tag{11}$$

For $\hat{V}_s \neq 0$, (10) defines a hyperbola, and because $A + C = 0$, this hyperbola is a rectangular one. However, it is still difficult to find the (x, y) pairs that satisfy both (9) and the unit circle. In order to make this possible, the hyperbola can be rotated in the position where the asymptotes are parallel to the Cartesian xy-axes. It is to be kept in mind that the final result obtained from this procedure has to be rotated back to the initial position, in order to obtain the actual arguments for the minima and maxima of (7).

Let us define (x', y') the coordinates of the points belonging to the hyperbola $H(x, y)$ after rotation. If the clockwise-rotation matrix is used, then

$$\left[\begin{array}{c} x\\ y \end{array}\right] = \left[\begin{array}{cc} \cos\gamma & \sin\gamma\\ -\sin\gamma & \cos\gamma \end{array}\right]\left[\begin{array}{c} x'\\ y' \end{array}\right], \tag{12}$$

which for

$$\gamma = \frac{1}{2}\arctan\frac{A}{B} \tag{13}$$

turns (10) into

$$\begin{aligned} H_{\rm rot}(x', y') =& 2\left(A\sin 2\gamma + B\cos 2\gamma\right)x'y'\\ &+2\left(D_{u,l}\cos\gamma - E_{u,l}\sin\gamma\right)x'\\ &+2\left(D_{u,l}\sin\gamma + E_{u,l}\cos\gamma\right)y' = 0. \end{aligned} \tag{14}$$

This is still a rectangular hyperbola, with the asymptotes oriented in parallel with the xy-axes. The nice thing with this form is that (14) can be expressed as $y' = y'(x')$, like

$$\begin{aligned} y' = y'(x') = -\frac{D_\gamma}{B_\gamma x' + E_\gamma}x', \\ x' \neq -\frac{E_\gamma}{B_\gamma}(= \text{asymptote}), \end{aligned} \tag{15}$$

where

$$\left\{\begin{array}{l} B_\gamma = A\sin 2\gamma + B\cos 2\gamma\\ D_\gamma = D_{u,l}\cos\gamma - E_{u,l}\sin\gamma\\ E_\gamma = D_{u,l}\sin\gamma + E_{u,l}\cos\gamma \end{array}\right\}. \tag{16}$$

C. Algebraic Solution

Returning to the initial aim of the analysis, we need to find the points that $H_{\rm rot}$ is crossing the unit circle, or equivalently, the points that the distance of $H_{\rm rot}$ from the origin is 1. The distance of the points that belong to $H_{\rm rot}$ from the origin is defined as

$$D_0(x') = \sqrt{x'^2 + y'^2(x')} = 1. \tag{17}$$

Therefore,

$$\begin{aligned} B_\gamma^2 x'^4 + 2B_\gamma E_\gamma x'^3 + \left(D_\gamma^2 + E_\gamma^2 - B_\gamma^2\right)x'^2\\ - 2B_\gamma E_\gamma x' - E_\gamma^2 = 0. \end{aligned} \tag{18}$$

Equation (18) is a $4^{\rm th}$-order polynomial and the roots of it have analytical expressions. This is in agreement with the previous indication that there are up to four extrema in the available-arm-energy margin expression in (7). The analytical expressions for the roots of a $4^{\rm th}$-order polynomial equation will not be presented here; it is only to be noted that out of the $x'_{1,2,3,4}$ roots, the ones that are of interest here are, of course, the real ones, which belong to the group

$$x'_{1,2,3,4} \in [-1, 1]. \tag{19}$$

The nice feature of this algorithm is that, as the solutions have analytical expressions, the algorithm can be applied online, with limited requirements on computational resources. All that is needed is to evaluate the parameters in (16) and apply them into the general expressions for the roots of (18). Online calculation is actually necessary in case of a drive system, where the exact parameters decided by a feedback controller may differ from the open-loop voltage and slip references that could be used for offline calculation. This effect will be made more clear in the following, when trying to confirm the arithmetic solutions with experimental results.

IV. Arithmetic Solutions and Experimental Results

Even though the analytical solution is general, and can be applied at any power or voltage level, the examples presented here are adapted to the laboratory setup, consisting of a low-voltage M2C prototype driving an 11-kW induction machine (IM). A photograph of the M2C prototype is shown in Fig. 3, the IM connected to a dc-generator load is shown in Fig. 4, and the ratings of the setup are given in Table I.

TABLE I
Ratings of the Experimental M2C and IM

Converter ratings		
Rated power	S	12 kVA
Number of submodules per arm	N	5
Carrier frequency	f_{car}	2.5 kHz
Input voltage	v_d	500 V
Submodule capacitor rated average voltage	$v^i_{cu,l0}$	100 V
Submodule capacitance	C	3.3 mF
Arm inductance	L	4.67 mH
Motor ratings		
Rated power	S	11 kW
Number of poles	N_p	4
Rated speed	n_r	1450 rpm
Stator line-line rated rms voltage	V_{l-l}	380 V
Rated rms phase current	I_s	23 A
Rated power factor	$\cos\varphi$	0.85

The control system is based on a digital signal processor (DSP), running a real-time operating system, and a field programmable gate array (FPGA) that handles the low-level control signals sent to the switches. The DSP is responsible for collecting analog measurements, such as voltages, currents, and rotor position, and also to run the current and internal converter control that generates the voltage reference for the M2C. This voltage reference is translated into switching actions in the FPGA and transmitted to all individual submodules.

Looking carefully in the ratings of this experimental setup, it becomes obvious that the prototype M2C cannot provide the full magnetization voltage that the IM requires at the rated-speed operation. For this reason, the base speed is defined here as the speed up to which the IM can be fully magnetized in this setup. Assuming that the peak-output voltage provided from the M2C cannot exceed 250 V, the machine can be fully magnetized only up to 80% of its rated speed, meaning that the base speed considered in these experiments is the speed of 1150 rpm.

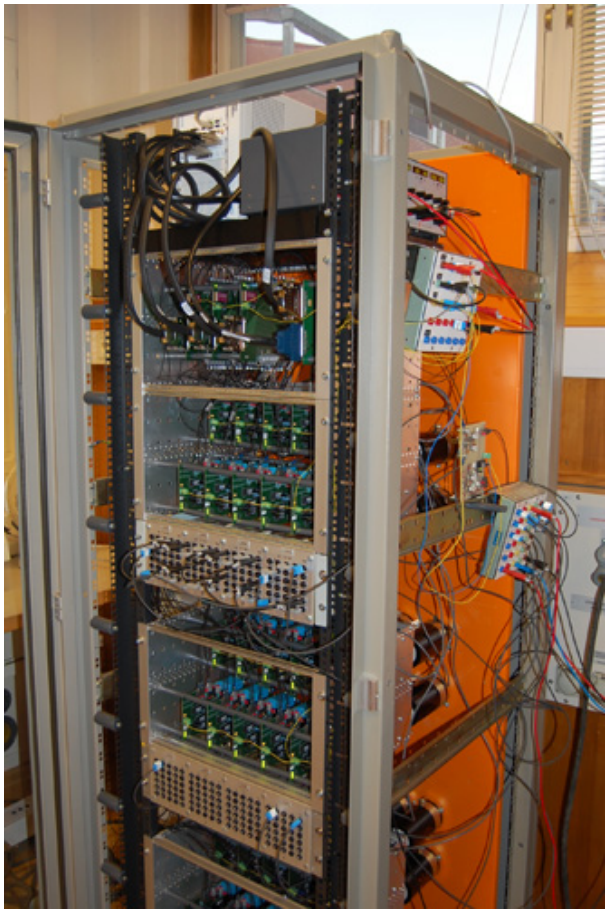

Fig. 3. Picture of the experimental prototype M2C.

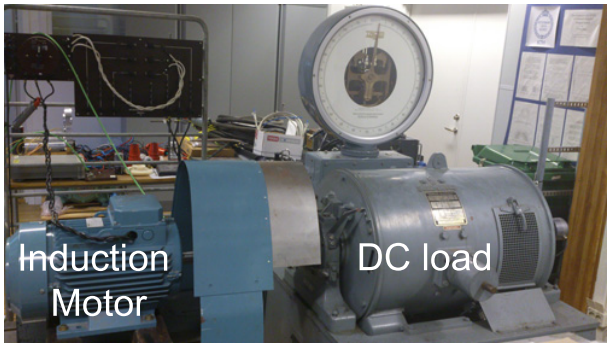

Fig. 4. Picture of the experimental 11-kW IM, connected to a dc-generator load.

A. Arithmetic Examples

A number of results for different operating points are provided in order to show the possibilities of using this optimization algorithm to estimate the average capacitor voltage. These arithmetic examples are calculated offline, based on the ratings of the downscaled lab setup, given in the Appendix. As long as all parameters are given, it is possible to calculate the following results even with a simple calculator that can

solve 4^{th}-order polynomial equations. In this case the Maple® software has been used, in order to draw the geometrical interpretation shown below.

In order not to lose the point with the geometrical interpretations of the optimization algorithm, the calculations and graphical representation of the equations are explained thoroughly only for one case. For the rest of the operating points only the final results are shown. All arithmetic operating points are evaluated with the rated current for the machine, and for the rated power factor that will provide the rated torque. The phase voltages and the stator frequencies applied to evaluate four different cases, along with the resulting average capacitor voltages are given in Table II.

TABLE II
VOLTAGES AND FREQUENCIES USED FOR ARITHMETIC EXAMPLES

	Case 1	Case 2	Case 3	Case 4
n_r [rpm]	1150	900	700	500
ω_s [rad/s]	$2\pi 40$	$2\pi 31.67$	$2\pi 25$	$2\pi 18.33$
$\hat{V}_s$ [V]	250	200	155	114
$v^i_{cu,l0}\|_{\min}$ [V]	94	84	77	78

Algorithm Steps (Case 3): This is the case representing a speed that is already below 50% of the rated speed for the IM. A graphical representation of (10), when substituting the parameters from (11) that correspond to this case is shown in Fig. 5 in red. Applying an anti-clockwise rotation, i.e, $\gamma = -0.537$, the rotated curve described by (14) is shown in green, while the unit circle is shown in blue. The parameters

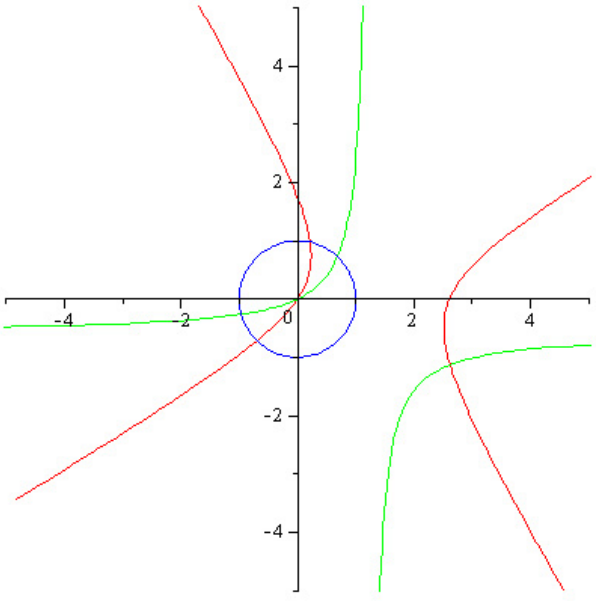

Fig. 5. Graphical representation of (10) [red curve], and the rotated position (14) [green curve], for the case of 700 rpm. The blue curve represents the unit circle $(x^2 + y^2 = 1)$.

in (16) can now be calculated from the position of the green curve, and (18) can be solved. The solutions of (18), i.e, the crossing points of the green curve and the unit circle are found to be

$$\begin{bmatrix} x'_1 \\ x'_2 \end{bmatrix} = \begin{bmatrix} -0.966 \\ 0.688 \end{bmatrix} \Rightarrow \begin{bmatrix} y'_1 \\ y'_2 \end{bmatrix} = \begin{bmatrix} -0.258 \\ 0.726 \end{bmatrix}. \quad (20)$$

Rotating back to the initial position that is represented by the red curve in Fig. 5, the $x - y$ coordinates are

$$\begin{bmatrix} x_1 \\ y_1 \end{bmatrix} = \begin{bmatrix} -0.698 \\ -0.716 \end{bmatrix}, \begin{bmatrix} x_2 \\ y_2 \end{bmatrix} = \begin{bmatrix} 0.219 \\ 0.976 \end{bmatrix}, \quad (21)$$

and after replaced into (7), the minimum possible average (i.e, $\Delta W_{cu,l}|_{\min} = 0$) becomes

$$W^{\Sigma}_{cu0}|_{\min} = 49 \text{ J}, \text{ or } v^i_{cu0}|_{\min} = 77 \text{ V}. \quad (22)$$

Getting back to the available energy margin as given in (7), and substituting the value estimated in (22), the margin can also be interpreted geometrically as (7) a quadratic equation in the $(\cos\theta, \sin\theta)$ coordinate system. As concluded from above, at the minimum value of the average capacitor voltage, i.e., 77 V, this expression should be tangent to the unit circle. It should be moving away for larger values of v^i_{cu0}, as e.g. the rated average of 100 V. Fig. 6 shows the two latter cases: the red curve represents the $v^i_{cu0}|_{\min}$ =77 V case, while the black curve represents the rated average capacitor voltage v^i_{cu0} =100 V.

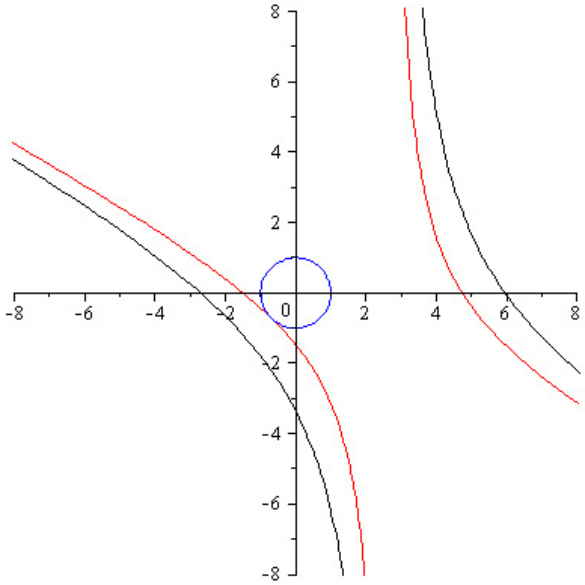

Fig. 6. 700 rpm case. Graphical representation of (7) for different values of v^i_{cu0}: 77 V [red curve], 100 V [black curve]. The blue curve represents the unit circle $(x^2 + y^2 = 1)$.

B. Experimental Verification

Depending on the exact machine and converter characteristics, as well as the motor controller function, the operating point may slightly differ from the one that is estimated in the arithmetic examples. The experiments are run using a current controller that adapts the converter voltage in such a way that creates current components at the output of the converter with the requested characteristics $(I_s, \cos\varphi)$. The rotor speed is controlled from the dc-load side, and kept

constant at the requested value. Therefore, the actual quantities ω_s and $\hat{V}_s$ are obtained as results of the operation, and cannot be considered as set-points. As a result, in order to verify the arithmetic examples shown above for the same rotor speed, the algorithm is run with parameters evaluated in run-time. The parameters used for the experimental cases, as well as the resulting average capacitor voltage for each case are given in Table III.

TABLE III
VOLTAGES AND FREQUENCIES USED FOR EXPERIMENTAL VERIFICATION

	Case 2	Case 3
n_r [rpm]	900	700
ω_s [rad/s]	$2\pi 31.30$	$2\pi 24.63$
$\hat{V}_s$ [V]	212	183
$v^i_{cu,l0}\|_{\min}$ [V]	87	81

Case 2 - 900 rpm: To start with, it may be interesting to investigate the waveforms of the stator quantities, i.e., the line-to-line voltages, and the phase currents. These are shown in Fig. 7, and it becomes obvious that the output quantities of the converter are not distorted by the reduction of the average capacitor voltage. The sum-capacitor voltage along with the inserted arm-voltage reference are shown in Fig. 8. This is the case with an average voltage as estimated by the algorithm, i.e., 87 V. The sum-capacitor voltage and the inserted arm voltage for the same operating point, when keeping the capacitor average voltage at its rated value, are shown in Fig. 9. In such a case, the peak of the capacitor voltage is unnecessarily high (15% higher compared to Fig. 8), as there is a lot of unused space below it, which will affect the converter-voltage rating.

Case 3 - 700 rpm: Similarly, for a lower speed, where the capacitor-voltage ripple is even greater, and the request for stator voltage is lower, the same methodology can be used. The output quantities are shown in Fig. 10. The sum-capacitor voltage and the inserted arm-voltage reference are shown in Fig. 11. It can be observed that the peak of the sum-capacitor voltage is not more than 500 V, while in the case of using the rated average of 100 V per capacitor, the same peak would approach almost 600 V, i.e., 23.5% higher voltage ratings than necessary, as shown in Fig. 12.

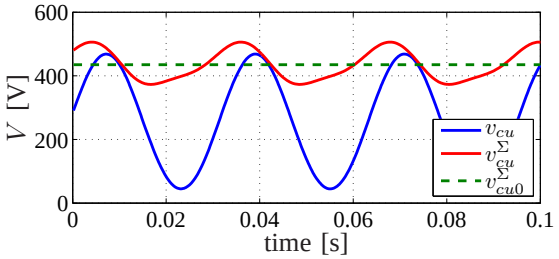

Fig. 8. Sum capacitor voltage and inserted arm voltage reference for the speed of 900 rpm, with an average capacitor voltage of 87 V.

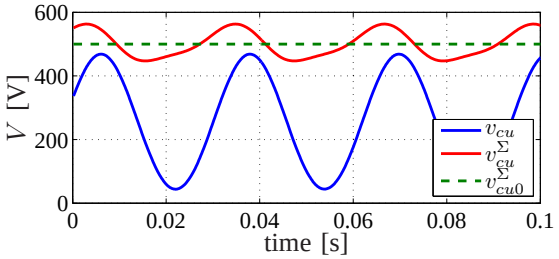

Fig. 9. Sum capacitor voltage and inserted arm voltage reference for the speed of 900 rpm, with an average capacitor voltage of 100 V.

V. DISCUSSION

The major advantage of this method is that there is no need for energy exchange between the arms to compensate for the increased energy pulsation in the capacitors [11], [12], as this is accommodated in another way. This is valuable and applicable in a wide range of frequencies below the base speed.

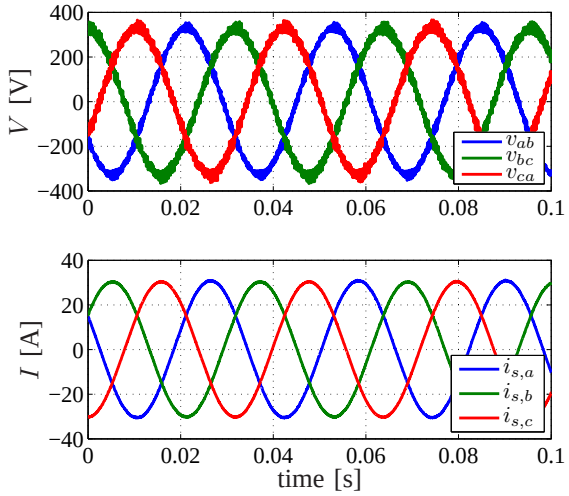

Fig. 7. Line-to-line stator voltage and stator current for the speed of 900 rpm.

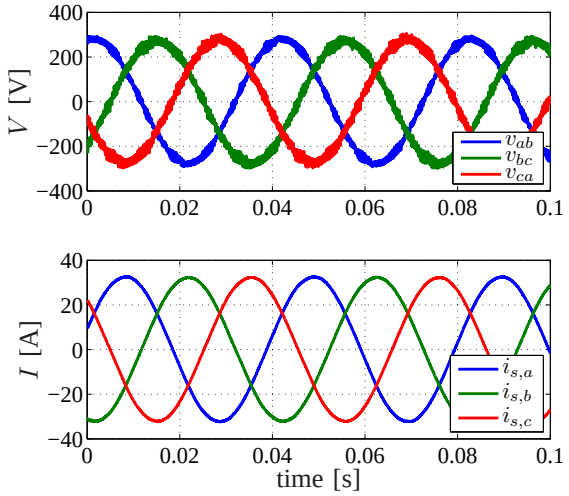

Fig. 10. Line-to-line stator voltage and stator current for the speed of 700 rpm.

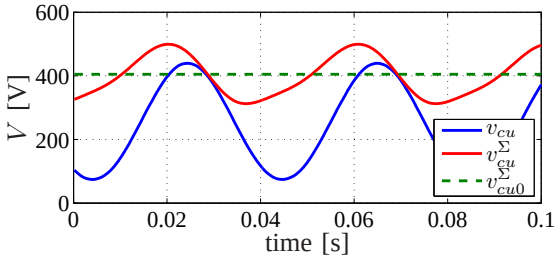

Fig. 11. Sum capacitor voltage and inserted arm voltage reference for the speed of 700 rpm, with an average capacitor voltage of 81 V.

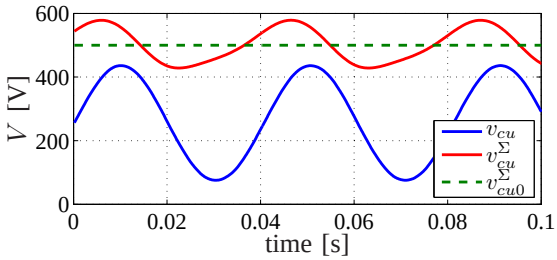

Fig. 12. Sum capacitor voltage and inserted arm voltage reference for the speed of 700 rpm, with an average capacitor voltage of 100 V.

Unlike [11]–[13], [15], neither additional oscillating components in circulating currents nor a common-mode voltage is required, and any overrating of the converter is, therefore, avoided.

Apart from the reduction in voltage ratings and the avoidance to increase the conduction losses with an oscillating circulating current, this method provides further significant advantages. A major one is that even when operating at a lower speed, where the required output voltage is small, all the available levels are used, as there is less voltage stored than the rated. The individual duty ratio of the semiconductors that insert the capacitors is consequently increased, and the lower the capacitor voltage is, the closer to unity the duty ratio becomes. The theoretical limit is when $V_s = 0$, the minimum capacitor voltage can be 50% of the rated average, for unity duty ratio in all the "insert" switches, as this will keep the dc-bus voltage constant. This operating point would be possible though only in case there is no output current. As soon as current starts flowing, it becomes impossible to operate the converter at this point due to the resulting capacitor voltage ripple. The fact that all the available levels are used, even when a lower stator voltage is requested, can be observed from the output-voltage waveforms shown in Fig. 7 and 10. In this sense the stator current is less distorted at lower speeds, compared to the case of having the rated voltage stored in the capacitors and switching within fewer levels. The reduced average capacitor voltage is, at the same time, the voltage that is switched on and off by the semiconductors. Assuming that the combination of the reduced capacitor voltage and the increased duty ratio will keep the current almost unaffected (except for the small improvement in its distortion), the switching losses are reduced, approximately by the reduction of the switched voltage [21], [22].

A consequence of this method is that operating with as little capacitor voltage as needed may limit the transient response of the drive, in case of a quick demand for torque above the rated. It is reasonable to think that the output-current controller may saturate, as there will not be any more available voltage. However, as pointed out in [19], the available total voltage in the capacitors is actually controlled by creating a temporary pulse in the circulating current. Apparently, the circulating current is required to have a quicker response than the output current, and as the dynamics of it are governed by the arm inductors, special consideration needs to be taken when deciding their size. A reasonably small value of arm inductance, combined with appropriate tuning of the two current controllers can give a system response of a few milliseconds in the output current, even for a torque demand above the rated.

At the same time, this analytical investigation can be used even when the stator-current requirement is lower. The parameters in (11) can actually be calculated for any operating point, irrespective of the frequency, the output power, or the current requirements, and the solution of the algorithm will give the optimal selection of the average capacitor voltage for every operating point, without the need to inject circulating current. Therefore, this method is not limited to applications where the torque request is the rated, as the cases shown experimentally in this paper, but it is more general, and can be applied in all applications involving M2Cs.

VI. Conclusions

This paper discusses an algorithm that provides the optimal selection of the average capacitor voltage for M2Cs. The solution is based on a geometrical interpretation that allows to formulate a polynomial equation, which has analytical solutions. Arithmetic examples for a certain M2C and IM setup are shown and experimentally confirmed. The algorithm presented here is very general and can be used in any application involving M2Cs, irrespective of the power/voltage level. The benefits of estimating the operating points with this method are that it does not cause any voltage or current overrating of the converter components, it does not increase the conduction losses, it decreases the switching losses, and it creates a very high-quality current waveform, even when the required output voltage is fairly small.

References

[1] A. Lesnicar and R. Marquardt, "An innovative modular multilevel converter topology suitable for a wide power range," in *Proc. IEEE Bologna Power Tech*, vol. 3, 2003.

[2] M. Glinka and R. Marquardt, "A new ac/ac multilevel converter family," *IEEE Trans. Ind. Electron.*, vol. 52, no. 3, pp. 662–669, Jun. 2005.

[3] N. Flourentzou, V. G. Agelidis, and G. D. Demetriades, "VSC-based HVDC power transmission systems: An overview," *IEEE Trans. Power Electron.*, vol. 24, no. 3, pp. 592–602, Mar. 2009.

[4] M. Winkelnkemper, A. Korn, and P. Steimer, "A modular direct converter for transformerless rail interties," in *Proc. IEEE Int Industrial Electronics (ISIE) Symp*, 2010, pp. 562–567.

[5] H. Akagi, "Classification, terminology, and application of the modular multilevel cascade converter (MMCC)," *IEEE Trans. Power Electron.*, vol. 26, no. 11, pp. 3119–3130, Nov. 2011.

[6] J. Huber and A. Korn, "Optimized pulse pattern modulation for modular multilevel converter high-speed drive," in *Power Electronics and Motion Control Conference (EPE/PEMC), 2012 15th International*, Sep. 2012.

[7] J. Ferreira, "The multilevel modular dc converter," *IEEE Trans. Power Electron.*, vol. 28, no. 10, pp. 4460–4465, Oct. 2013.

[8] M. Spichartz, V. Staudt, and A. Steimel, "Modular multilevel converter for propulsion system of electric ships," in *IEEE Electric Ship Technologies Symposium (ESTS)*, 2013, pp. 237–242.

[9] M. Hiller, D. Krug, R. Sommer, and S. Rohner, "A new highly modular medium voltage converter topology for industrial drive applications," in *Proc. 13th European Conf. Power Electronics and Applications EPE '09*, 2009, pp. 1–10.

[10] M. Hagiwara, K. Nishimura, and H. Akagi, "A medium-voltage motor drive with a modular multilevel PWM inverter," *IEEE Trans. Power Electron.*, vol. 25, no. 7, pp. 1786–1799, Jul. 2010.

[11] A. J. Korn, M. Winkelnkemper, and P. Steimer, "Low output frequency operation of the modular multi-level converter," in *Proc. IEEE Energy Conversion Congress and Exposition (ECCE)*, 2010, pp. 3993–3997.

[12] J. Kolb, F. Kammerer, and M. Braun, "Dimensioning and design of a modular multilevel converter for drive applications," in *15th International Power Electronics and Motion Control Conference (EPE/PEMC)*, Sep. 2012.

[13] A. Antonopoulos, L. Ängquist, S. Norrga, K. Ilves, and H.-P. Nee, "Modular multilevel converter ac motor drives with constant torque form zero to nominal speed," in *IEEE Energy Conversion Congress and Exposition (ECCE)*, Sep. 2012, pp. 739–746.

[14] K. Wang, Y. Li, Z. Zheng, and L. Xu, "Voltage balancing and fluctuation-suppression methods of floating capacitors in a new modular multilevel converter," *IEEE Trans. Ind. Electron.*, vol. 60, no. 5, pp. 1943–1954, May 2013.

[15] M. Hagiwara, I. Hasegawa, and H. Akagi, "Startup and low-speed operation of an adjustable-speed motor driven by a modular multilevel cascade inverter (MMCI)," in *IEEE Energy Conversion Congress and Exposition (ECCE)*, Sep. 2012, pp. 718–725.

[16] K. Ilves, A. Antonopoulos, L. Harnefors, S. Norrga, L. Ängquist, and H.-P. Nee, "Capacitor voltage ripple shaping in modular multilevel converters allowing for operating region extension," in *Proc. IECON 2011 - 37th Annual Conf. IEEE Industrial Electronics Society*, 2011, pp. 4403–4408.

[17] L. Ängquist, A. Antonopoulos, D. Siemaszko, K. Ilves, M. Vasiladiotis, and H.-P. Nee, "Open-loop control of modular multilevel converters using estimation of stored energy," *IEEE Trans. Ind. Appl.*, vol. 47, no. 6, pp. 2516–2524, Nov.-Dec. 2011.

[18] A. Antonopoulos, L. Ängquist, L. Harnefors, K. Ilves, and H.-P. Nee, "Global asymptotic stability of modular multilevel converters," *IEEE Trans. Ind. Electron.*, vol. 61, no. 2, Feb. 2014.

[19] A. Antonopoulos, L. Ängquist, and H.-P. Nee, "On dynamics and voltage control of the modular multilevel converter," in *Proc. 13th European Conf. Power Electronics and Applications EPE '09*, 2009, pp. 1–10.

[20] L. Harnefors, A. Antonopoulos, S. Norrga, L. Ängquist, and H.-P. Nee, "Dynamic analysis of modular multilevel converters," *IEEE Trans. Ind. Electron.*, vol. 60, no. 7, pp. 2526–2537, Jul. 2013.

[21] S. Allebrod, R. Hamerski, and R. Marquardt, "New transformerless, scalable modular multilevel converters for HVDC-transmission," in *Proc. IEEE Power Electronics Specialists Conf. PESC 2008*, 2008, pp. 174–179.

[22] T. Modeer, H.-P. Nee, and S. Norrga, "Loss comparison of different sub-module implementations for modular multilevel converters in hvdc applications," *EPE Journal*, vol. 22, no. 3, pp. 32–38, Sep. 2012.

Antonios Antonopoulos (S'06) was born in Athens, Greece, in 1984. He received the Diploma of electrical and computer engineering from the National Technical University of Athens, Greece in 2007, and his Licentiate degree in electrical engineering from the KTH Royal Institute of Technology, Stockholm, Sweden in 2011.

Between 2008–2014 he was a Ph.D. student at the Electrical Energy Conversion Laboratory (E2C) at KTH in Stockholm. Since 2014, he has been with ABB, at Corporate Research, Västerås, Sweden. His research interests include high-power-electronic converters for large- and medium-scale motor drives and grid applications.

Lennart Ängquist (M'06) was born in Växjö, Sweden, in 1946. He received the M.Sc. degree from the Lund Institute of Technology, Lund, Sweden, in 1968 and the Ph.D. degree from the KTH Royal Institute of Technology, Stockholm, Sweden, in 2002.

He has been employed by ABB (formerly ASEA), Västerås, Sweden, working as a development engineer first in the Corporate Research high power laboratory, then in the Drives department from 1974 to 1987, in the Relay department in 1988 and finally in the FACTS division, where he became a Senior Specialist in Power Electronics, from 1988 to 2008. He was active in the early development of the modern asynchronous motor drives in ABB for industrial and traction applications, both with respect to main circuits as well control systems based on the field-oriented approach. In the FACTS division his main work was related to development of Thyristor Controlled Series Capacitors (TCSC) and with the installations in Stöde, Sweden, for mitigation of sub-synchronous resonance and in Imperatrìz, Brazil, for power oscillation damping. He was an Adjunct Professor at KTH from 2004 to 2010 where he is still employed as a researcher. His research interests include application of high-power electronic apparatus, specifically modular multilevel converters, in electrical transmission system, mainly with respect to modeling and simulation.

Lennart Harnefors (S'93–M'97–SM'07) was born in 1968 in Eskilstuna, Sweden. He received the M.Sc., Licentiate, and Ph.D. degrees in electrical engineering from the KTH Royal Institute of Technology, Stockholm, Sweden, and the Docent degree in industrial automation from Lund University, Lund, Sweden, in 1993, 1995, 1997, and 2000, respectively. Between 1994–2005, he was with Mälardalen University, Västerås, Sweden, where he held the positions of Research Assistant, Senior Lecturer, and, from 2001, Professor. He served as Head of the Systems, Control, and Power Engineering Laboratory 1998–2004. Between 2001–2005, he was, in addition, a part-time Visiting Professor of electrical drives with Chalmers University of Technology, Göteborg, Sweden. Since 2005, he has been with ABB, where he served in various capacities at the Grid Systems/HVDC business unit 2005–2012. Currently, he is a Senior Principal Scientist at Corporate Research, Västerås, Sweden. He is part time with KTH as an Adjunct Professor of power electronics. His research interests include analysis and control of power electronic systems, particularly grid-connected converters and ac drives.

Prof. Harnefors was the recipient of the 2000 ABB Gunnar Engström Energy Award and the 2002 IEEE TRANSACTIONS ON INDUSTRIAL ELECTRONICS Best Paper Award. He is an Associate Editor of the IEEE TRANSACTIONS ON INDUSTRIAL ELECTRONICS, a member of the Editorial Board of *IET Electric Power Applications*, and a member of the Executive Council and the International Scientific Committee of the European Power Electronics and Drives Association (EPE). He is the author of more than 100 papers and holds five granted patents with several more pending.

Hans-Peter Nee (S'91–M'96–SM'04) was born in Västerås, Sweden, in 1963. He received the M.Sc., Licentiate, and Ph.D degrees in electrical engineering from the KTH Royal Institute of Technology, Stockholm, Sweden, in 1987, 1992, and 1996, respectively. In 1999, he was appointed Professor of power electronics at KTH, where he currently serves as the Head of the Electrical Energy Conversion Laboratory. His current research interests include power electronic converters, semiconductor components, and control aspects of utility applications, such as flexible ac transmission systems and high-voltage dc transmission, and variable-speed drives.

Prof. Nee was the recepient of the Energy Prize by the Swedish State Power Board in 1991, the ICEM'94 (Paris) Verbal Prize in 1994, the Torsten Lindström Electric Power Scholarship in 1996, and the Elforsk Scholarship in 1997. He is a member of the European Power Electronics and Drives Association (EPE), involved with the Executive Council and the International Scientific Committee. He is also an Associate Editor of the IEEE TRANSACTIONS ON POWER ELECTRONICS and was on the board of the IEEE Sweden Section for several years, serving as its Chairman during 2002-2003.